ACS OMEGA

http://pubs.acs.org/journal/acsodf

Article

Novel Electrochemical Sensing of Catechins in Raw Green Tea Extract via a Trimetallic Zeolitic Imidazolate Fibrous Framework

Thatchanamoorthy Thenrajan,[¥] Sam Sankar Selvasundarasekar,[¥] Subrata Kundu,* and Jeyaraj Wilson*

Cite This: *ACS Omega* 2022, 7, 19754−19763

Read Online

ACCESS | Metrics & More | Article Recommendations | Supporting Information

ABSTRACT: Human health-related issues are increasing in day to day life because of the modern and unhygienic food lifestyles. In recent times, green tea (GT) gains more attention due to its numerous health benefits. It contains more biologically active compounds that improve mental health, increase metabolism, reduce cancer risks, and serve as an anti-aging agent for the brain. As it is globally consumed, the evaluation of the compounds present in it is very important. Hence, an attempt has been performed to evaluate these components in GT by using a cobalt nickel iron-based trimetallic zeolitic imidazolate framework as microfibers (CoNiFe-ZIF-MFs) synthesized via an electrospinning technique. Interestingly, the synthesized CoNiFe-ZIF-MFs catalyst simultaneously detects three major catechin (CT) groups, namely, epigallocatechin-3-gallate (EGCG), epicatechin (EC), and epicatechingallate (ECG). Further, the square wave voltammetry findings showed that there is a wide linear range of 50 ng to 1 mg for all the three CTs with LODs 45, 8, and 4 ng for EGCG, EC, and ECG, respectively. These results confirm the excellent sensing behavior of the composite toward GT extracts, proposing its practical utility in real-time compound analysis in food sectors. Other results like stability and reproducibility also promote its usage in the biomedical field. This study mainly focuses on the direct sensing of CTs present in GT without spiking any commercially purchased sample, and the sensing was performed simultaneously for all the three analytes; thus, this work gains novelty from the existing ones.

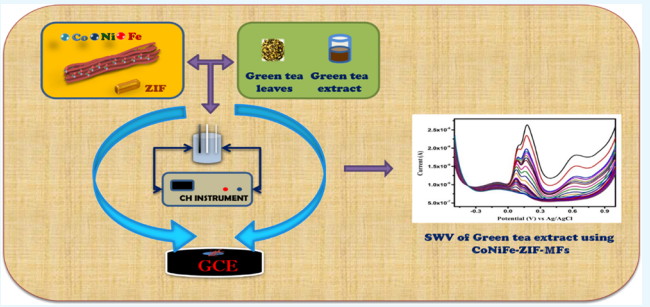

1. INTRODUCTION

Currently, green tea (GT) has emerged as a healthy drink owing to its benefit to the human body. Its valuable features are mainly due to the presence of various chemical compounds such as catechins (CTs), antioxidants, vitamins, and amino acids. In particular, CT is the main compound from tea leaves that possess intensive anti-oxidants, which leads to the enhancement of physiological activities, i.e., preventing or reducing skin damage. It is one of the members of polyphenol groups, seen in various medicinal plants. The major sources of CTs are *Camellia sinensis* (*C. sinensis*) and *C. assumica*. The composition of GT is 75−80% water and polyphenol compounds. Their structure includes major amounts of hydroxyl groups (−OH) and can be easily combined with other materials for composite formation. In addition to that, six types of CTs, namely, CT, epicatechin (EC), epicatechingallate (ECG), epigallocatechin, epigallocatechin gallate (EGCG), and gallocatechingallate, are prominently present in GT. They provide various advantages to the human body by free radical scavenging and retardation of the degrading extracellular matrix. Because of the hydroxyl groups, they can show more antioxidant activity compared with other standard anti-oxidants.[1] Recently, it is observed that the polyphenol CTs present in GT have the ability to inhibit corona virus and reduce the lung infection in mice.[2] The chemical components present in GT and the different degree of oxidative polymers formed by CTs play a decisive role in determining the properties of GT. Therefore, using this as a chemical index, it is possible to validate the quality of GT. Up to date, high-pressure liquid chromatography,[3−6] fluorescence spectroscopy,[7,8] chemiluminescence,[9] and optical methods[10] are involved in the GT sensing with excellent results. But, the high instrumentation cost, pre-sample preparation, complicated methods, and numerous chemical usage create a necessity to find easy and cheap alternative sensing method.

Many efforts have been made to develop an alternative analytical method with exceptional advantages. The need of empirical growth on the surroundings and the society can be achieved in the improvement of safety, controlled monitoring, quality management, and diagnosis. Compared with the other analytical methods indicated so far, the electrochemical technique is found to be more attractive due to the satisfaction

Received: March 15, 2022
Accepted: May 27, 2022
Published: June 3, 2022

https://doi.org/10.1021/acsomega.2c01536
ACS Omega 2022, 7, 19754−19763

of such demands. The notable advantages of electrochemical biosensors are their technical simplicity, high sensitivity, easy adaptability for rapid and on-spot analysis, and low-cost devices.[11] So, this work is mainly focused on the electrochemical method of bio-sensing.

In electrochemical sensors, the role of materials is of high importance. Previously, various materials have been reported for the detection of CTs in GT products. An enzymatic biomimetic sensor based on a novel copper(II) complex was developed for the detection of CT in GT using a capillary electrophoresis method. Here, they used a ligand with copper for the effective binding of CTs, which resulted in a wide range of 4.95×10^{-6} to 3.27×10^{-5} mol L^{-1} and a detection limit of 2.8×10^{-7} mol L^{-1}.[1] Similarly, by immobilizing 2,2′-(1,4-phenylenedivinylene)bis-8-hydroxyquinoline (PBHQ) on TiO_2, an optical sensor was proposed for the CT sensing.[10] Molecularly imprinted polymer (MIP) electrodes and non-imprinted polymer electrodes were developed and used for the effective sensing of CTs in tea samples.[12] Interestingly, using the electrochemical method, a non-enzymatic sensor using the MIP with $Ni(OH)_2$ nanopetals for the selective determination of EGCG was fabricated. The proposed sensor presented excellent results with commercially obtained EGCG with an LOD of 7 nM, which was finally verified with the GT samples.[13] Recently, metal−organic frameworks (MOFs) attract the attention of researchers due to their notable characteristics like huge surface areas, unique pore interiors, and simple functionalization procedures in various fields such as sensors, catalysis, gas storage, and molecular separations.[14] A subclass of MOFs is zeolitic imidazolate frameworks (ZIFs), a broad class of composite materials wherein a metal ion is coordinated with the desired organic ligands that form a kind of framework through coordination bonds. The arrangement of ZIFs has regular pores for the binding of the target analytes and has the potential to evaluate the species even at the molecular level. In addition, the unique properties of ZIFs are suitable for the surface immobilization of biorecognition units and electrocatalysts because of their surface area, presence of more functional groups (C, H, and N), and high chemical stability. Owing to this excellent nature, ZIFs are widely utilized in various fields such as energy storage, sensors, chromatographic separation, etc. To date, monometallic and bimetallic ZIF-based composites are explored using some transition metal ions (Co, Ni, Fe, and Zn) in the field of electrochemical biosensors. In comparison, the latter one shows good sensing results, mainly due to the synergism between two metal ions, which provides better stability and selectivity. The catalytic movement and degrees of freedom are increased with the addition of more than one metal ion along with their superior performance. From the above discussion, it is believed that the trimetallic ZIF composites have outstanding electrocatalytic activity compared to the bimetallic and monometallic ones.[15] Increasing the number of metal ions on the ZIF matrix not only enhances the overall electrical conductivity but also gains advantages for better mechanical properties. Compared with the other methods, in terms of simplicity of procedures for operation and ease of handling, the electrospinning (ES) technique gains more attraction over the others. Generally, the fibrous materials produced by the ES technique are used in many applications including defense, biomedicine, tissue engineering, filtration, and protective clothing.[16]

Considering all the aforementioned details, we have synthesized a trimetallic cobalt, nickel, and iron ZIF (CoNiFe-ZIF)-based fibrous material for an effective sensing of CTs in the raw form of GT. So, the trimetallic CoNiFe-ZIF microfibrous (MFs) material is prepared by wet chemical and electrospinning techniques. The obtained GT extracts are directly used as an analyte for the electrochemical sensing process. The trimetallic CoNiFe-ZIF-MFs provided necessary interaction with the three CTs of the GT extract. To the best of our knowledge, no attempt to use a raw GT sample as an analyte for sensing through an electrochemical method was reported. It is observed that, normally, different CTs were bought commercially and tested by spiking the raw GT samples for practical utility. But, in this work, we have demonstrated the entire work using raw GT extract without any spiking of commercially available CTs. The detected CTs were compared with the commercially purchased samples for their confirmation and used for further studies.

2. EXPERIMENTAL SECTION

2.1. Instrumentation. The ES was performed by an ESPIN from PECO. Using a Bruker AXS D8 advanced diffractometer, X-ray diffraction studies were conducted. To analyze the surface morphology (FESEM), a SUPRA 55 Carl Zeiss was used. Various modes of vibration of the composite material were investigated via Raman spectroscopy using a model Raman spectrometer (SEKI Japan). X-ray photoelectron spectroscopy (XPS) analysis was performed by a Thermo Fisher Scientific, ESCA Lab 250. Other experimental electrochemical measurements such as cyclic voltammetry (CV), electrochemical impedance spectroscopy (EIS), and square wave voltammetry (SWV) were conducted using a CHI 6005D electrochemical workstation (CH Instruments, USA).

2.2. Materials and Reagents. Cobalt chloride, 2-methylimidazole, iron chloride, dimethyl formamide (DMF), nickel chloride, and polyacrylonitrile (PAN) were obtained from Sigma-Aldrich Co. Ltd., Bangalore (India). Epigallocatechin gallate (EGCG), epicatechin (EC), and quercetin were purchased from TCI Chemicals Co. Ltd., Bangalore (India). All the chemicals were of analytical grade and employed without any further purification. Ethanol was utilized as a solvent, and for the electrochemical measurements, phosphate buffer solution (PBS) was used as a supporting electrolyte. The preparation of PBS was as follows: sodium dihydrogen phosphate and disodium hydrogen phosphate were added to certain amounts of water in a beaker and stirred well together for complete dilution. Then, the pH was checked and adjusted accordingly to our desired levels by adding hydrochloric acid or sodium hydroxide. The electrochemical measurements were conducted in a three-electrode system. As a reference electrode, silver/silver chloride (Ag/AgCl) was used, and platinum (Pt) wire was chosen for a counter electrode. For the working electrode, a glassy carbon electrode (GCE) was used. Green tea (GT) leaves were purchased from the local market.

2.3. Synthesis of CoNiFe-ZIF Powder. To prepare the CoNiFe-ZIF powder, a simple wet chemical strategy was used. The three metal (cobalt, iron, and nickel) chloride precursors were taken in an equimolar ratio (1:1:1) and dissolved individually on a beaker containing 50 mL of ethanol. Similarly, 0.8 M 2-methylimidazole was solvated in a different beaker by using ethanol (beaker II). All the three metal solutions were mixed together under constant stirring for 30 min (beaker I). The obtained solution was added dropwise to

https://doi.org/10.1021/acsomega.2c01536
ACS Omega 2022, 7, 19754−19763

Scheme 1. Possible Mechanism for the Sensing of the Three CTs in GT Extract by CoNiFe-ZIF-MFs

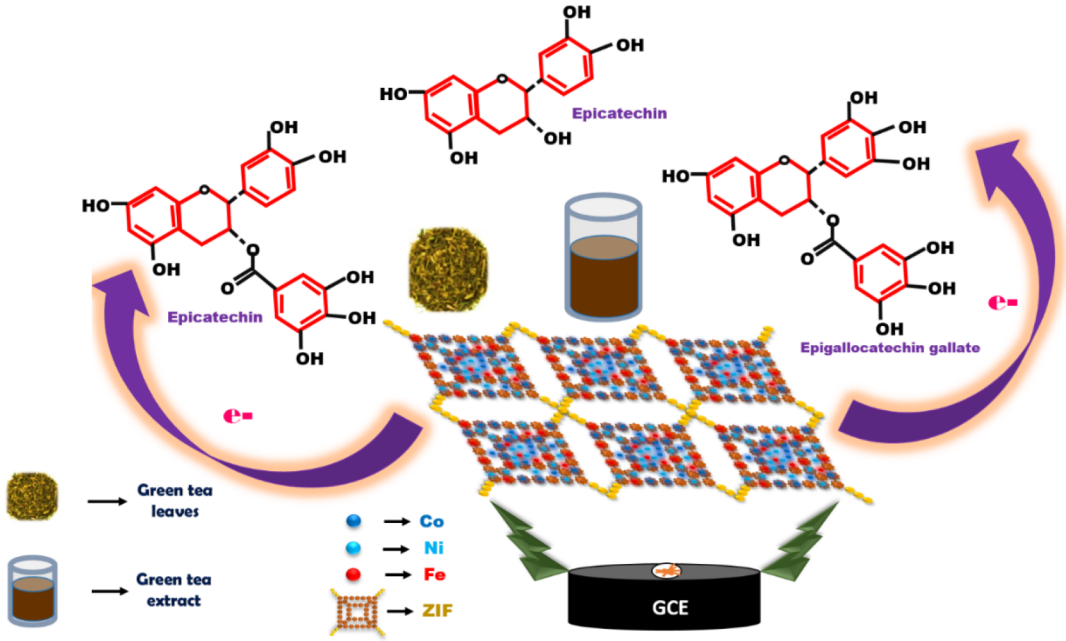

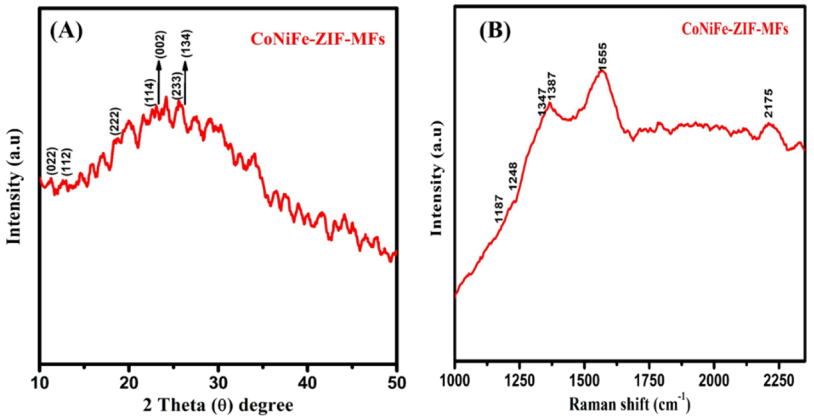

Figure 1. (A) XRD and (B) Raman studies of CoNiFe-ZIF-MFs.

beaker II solution and mixed well using a magnetic stirrer for a period of 2 h. During this period, a brown colored precipitate formed. Further, it is centrifuged and washed several times with water and ethanol to eliminate the unreacted compounds. Next to that, the resultant product was kept in an oven for 12 h at 70 °C. Finally, a brown colored powder was obtained, stored, and used for other process.

2.4. Synthesis of CoNiFe-ZIF Fibers. The as-prepared CoNiFe-ZIF powder was mixed with 2 mL of DMF followed by sonication to get a homogeneous mixture for the preparation of the material for the ES process. PAN was added as the polymeric source. The sample was kept stirring for 12 h to ensure the complete mixing of the elements present in it. Optimizing the desired parameters for fiber formation, the prepared sample was subjected to the ES instrument. The specifications are as follows: applied voltage, 18 kV; flow rate, 0.3 mL/h; distance amid the tip and collector, 12 cm; and a flat-type collector was used. In these described setups, the expected fibers were formed. Further, the prepared fibers were heated at 60 °C for 6 h using a box furnace for complete drying. Finally, CoNiFe-ZIF-MFs were formed and used for all the studies.

2.5. Experimental Conditions. All the experimental conditions are as follows: 10 mL of 0.1 M KCl in $[Fe(CN)_6]^{3-/4-}$ solution was used as an electrolyte. The SWV, pH, variations, stability, reproducibility, and CV in PBS were executed with a PBS electrolyte. All the studies were performed at a scan rate of 50 mV/s except for different scan rate studies conducted at 10−100 mV/s. The possible mechanism of the composite analyte interaction is given in Scheme 1 below.

3. RESULTS AND DISCUSSION

3.1. Material Characterizations. *3.1.1. XRD and Raman Studies.* In order to confirm the material formation, CoNiFe-ZIF-MFs is investigated by XRD analysis and the resultant pattern is shown in Figure 1A. The occurrence of cobalt ions on the ZIF matrix is depicted by the peaks at 12.35, 18, 25, and 26° representing the planes (112), (222), (233), and (134), respectively. Similarly, the addition of Fe ions onto the above is exhibited by a peak around 22.5° having a plane value of (114). This confirms that both Co and Fe ions are present, which is in

https://doi.org/10.1021/acsomega.2c01536
ACS Omega 2022, 7, 19754−19763

accordance with our previous literature.[17] Similarly, the presence of the Ni ions can also be depicted by the peaks at 11 and 23° having plane values of (022) and (002), which is well supported by our previous work.[18] These results clearly confirmed that all the three metal ions in the ZIF network attained a more appropriate coordination during the synthesis process. The decrease in the intensity of the peaks may be due to the usage of polymeric materials for composite preparation. This polymeric material has masked the formation of crystallinity.[19,20] As a result, the reduction of peak current was observed for CoNiFe-ZIF-MFs in the CV images (Section 3.2.1).

The vibration modes of the composite are investigated by the Raman spectra shown in Figure 1B. Peaks seen at 1347 and 1555 cm^{-1}correspond to the strong vibrations of the C−N stretching and methyl bending of the Co ion and imidazolate ZIF fibers, respectively. Incorporation of Fe and Ni metal ions in this network is confirmed by the 1187, 2175, 1387, and 1248 cm^{-1} peaks.[17,18] All these individual peaks strongly confirmed the coordination of metal ions with the ZIF and polymeric fibers through physical interaction.[21]

3.1.2. Fluorescence Studies. To analyze the fluorescence property, the system is subjected to fluorescence sensing with and without the analyte (Figure 2). Pure DI water is used as

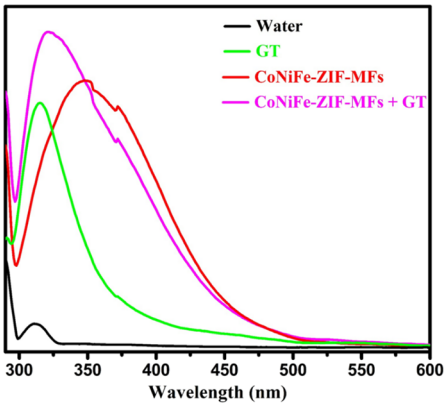

Figure 2. Fluorescence spectra of CoNiFe-ZIF-MFs and GT.

the solvent. The excitation wavelength is fixed at 280 nm where the emission of CTS is observed. For the bare GCE, a peak at 330 nm is a result of the Raman spectra of water. The GT sample showed an increased emission peak on the nearer wavelength, confirming its fluorescence behavior, due to the presence of CTs.[8]

Similarly, a broad peak with slight shift is seen for the CoNiFe-ZIF-MFs composite around 355 nm attributed to the $\pi^*-\pi$ transition of 2-methylimidazole in the ZIF matrix.[22] Interestingly, the composite in the presence of the GT extract showed a high intensity peak around 323 nm as a result of the π^* to n or a π^* to π transition combined with the fluorescence effect. The peak shift observed on the composite is mainly due to the interaction between the CTs and 2-methylimidazole. Moreover, the trimetallic nature of the ZIF greatly contributes to the fluorescence behavior of the composite. The high electron transfer of the trimetallic material greatly influences the effective interaction between the analyte and the composite material.[23] These results confirm the fluorescence nature of the composite with the analyte, which also indicates that CoNiFe-ZIF-MFs has excellent optical properties.

3.1.3. Morphology Analysis. The morphological aspects of CoNiFe-ZIF-MFs are confirmed by FESEM analysis where the fibrous structure is identified. At a low magnification of 10 μm, the fiber nature of the synthesized catalyst is indicated. It clearly depicts that the structural uniformity is highly maintained on the observed fibers. The size of the observed fibers evidently falls on the micro-regime. The CoNiFe-ZIF particles are randomly situated on the surface of the fiber network (Figure 3C,D). Also, the porous nature of the ZIF

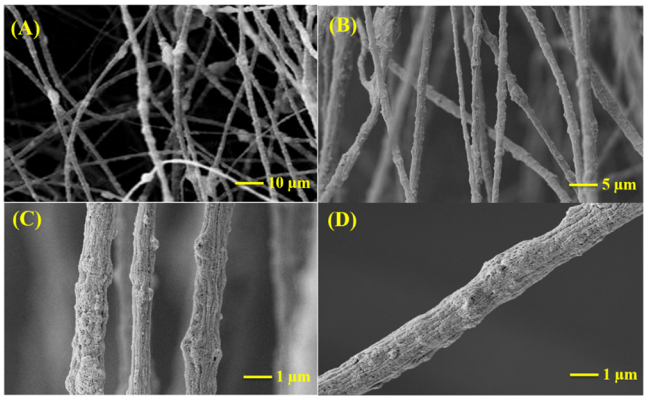

Figure 3. (A−D) SEM images of the CoNiFe-ZIF-MFs at various magnifications.

fibers is clearly visible in Figure 3D. So, the coordination of the ZIF network with the polymeric matrix and the fibrous structure is highly confirmed through the FESEM images. Since GT contains more than one compound, it can provide more possible interaction with an analyte.[24] In addition to this, the high surface area and porous nature of CoNiFe-ZIF-MFs are very much useful in binding with the target analyte, thereby increasing the material sensing behavior.[25,24]

3.1.4. XPS Spectra. In order to know the chemical nature of the as-synthesized CoNiFe-ZIF-MFs catalyst, XPS analysis is performed and the related results are shown in Figure 4A−F. The high-resolution XPS spectrum of Co 2p was recorded, and the results are seen in Figure 4A. The observed binding energy values 779.4, 782.5 and 785.5, 797.5 eV correspond to $2p_{3/2}$ and $2p_{1/2}$ along with their shake up peaks, respectively. It is observed that cobalt is present in the +2 oxidation state. In addition to that, the Ni 2p XPS plot also shows binding energy values of 853.9, 859.9 and 871.4, 878.3 eV, which correspond to $2p_{3/2}$ and $2p_{1/2}$ and related shake up peaks, respectively (Figure 4B). Similarly, the elemental state of nickel was identified as +2. Further, the XPS spectrum of Fe 2p was recorded and is shown in Figure 4C, wherein the observed binding energy values of 709.2, 714.2 and 723.2, 731.4 eV represent $2p_{3/2}$ and $2p_{1/2}$, respectively. The observed binding energy values well signified that the iron ion was predominantly present in the +3 state. So, the metallic state of Fe^{3+} was highly anticipated and effectively participated in the sensing process. Compared with the transition metal ions, the Fe ions have high electrochemical activity in terms of their smaller activation energies, low band gaps, higher charger density, and thermal activation at room temperature. So, this Fe ion must be involved in the interaction with the target biomolecule for producing excellent sensing results.[26] Also, in the C 1s XPS spectrum (Figure 4D), the functionalities such as C−OH, O−C═O, and C═O were observed at the binding energy values of 282.4, 283.2, and 284.4 eV, respectively.

https://doi.org/10.1021/acsomega.2c01536
ACS Omega 2022, 7, 19754−19763

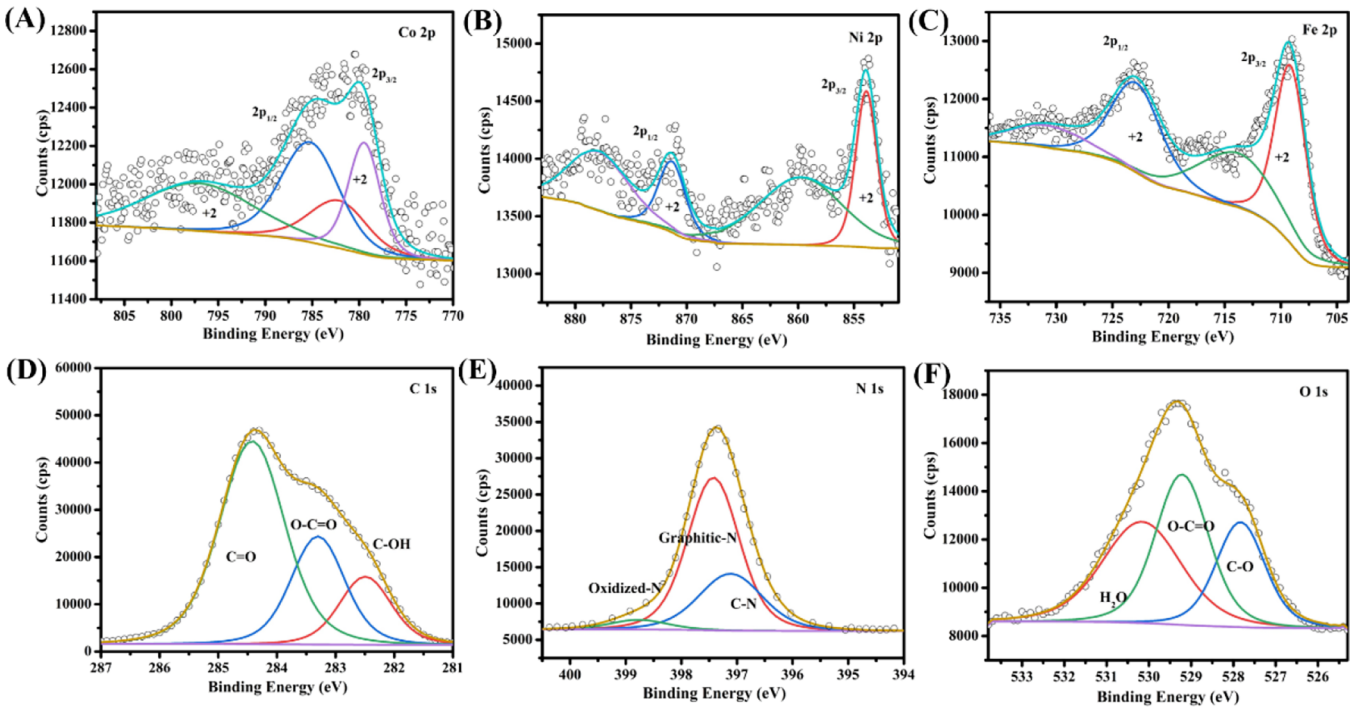

Figure 4. High-resolution XPS spectra of the CoNiFe-ZIF-MFs catalyst: (A−F) Co 2p, Ni 2p, Fe 2p, C 1s, N 1s, and O 1s plots, respectively.

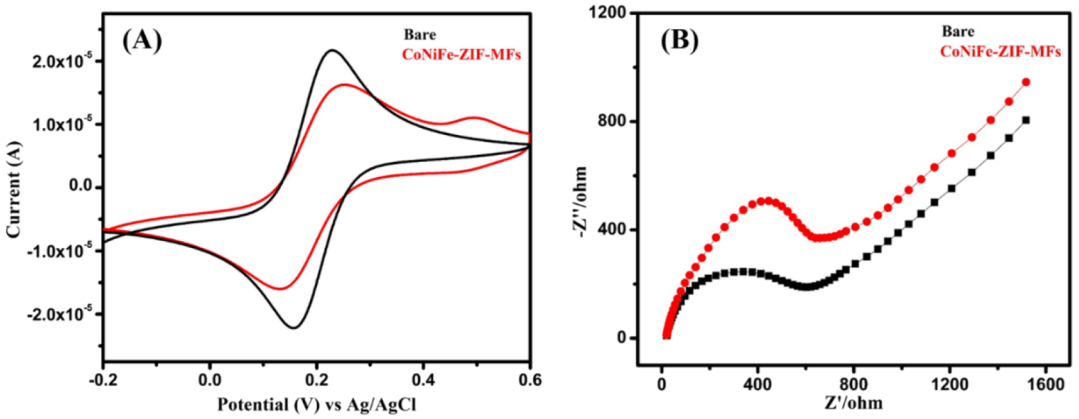

Figure 5. (A) CV and (B) EIS measurements of CoNiFe-ZIF-MFs.

In the case of the N 1s XPS spectrum, the observed functionalities are C−N, graphitic-N, and oxidized-N at the binding energy values of 397.0, 397.6, and 398.7 eV, respectively (Figure 4E). Finally, the functionalities of O 1s such as C−O, O−C═O, and H_2O were found with the binding energy values of 527.8, 529.2, and 530.1 eV, respectively (Figure 4F). Hence, the chemical nature of all the elements and their oxidation states were well identified in the ZIF hybrid.

3.2. Electrochemical Studies. *3.2.1. CV, EIS, and Scan Rate Measurements of CoNiFe-ZIF-MFs in* $[Fe(CN)_6]^{3-/4-}$. The electrical conductivity of the composite is evaluated using a CV study shown in Figure 5A. According to the results obtained, the composite CoNiFe-ZIF-MFs exhibited a minimum peak current value (1.61×10^{-5} A) compared with the unmodified GCE (2.17×10^{-5} A). This is due to the effect of PAN usage for the fiber formation, which reduces the redox process in the $[Fe(CN)_6]^{3-/4-}$ solution. Generally, the Fe ions exhibit a high electronic conductivity of five orders of magnitude higher than the other transition metal ions in the MOFs structure.[26] So, these Fe ions must be almost involved in the electrochemical interaction with the electrolyte. On the other hand, the electrolyte used here also contains similar charged ferrous ions, which create electrostatic repulsion, leading to the reduction in peak current value. So, the resulting current value is lower than that of the bare GCE. The redox peak potential difference (ΔE_p) values are 73 mV for the bare GCE and 119 mV for the CoNiFe-ZIF-MFs-modified GCE. The composite shows a two-electron transfer, indicating its redox process.[27] All these results correspond to the primary peak of CoNiFe-ZIF-MFs obtained at a potential value of 0.24 V, while the secondary peak at 0.49 V may be due to the oxidation of other metal ions (Co^{2+} and Ni^{2+}) in the composite, indicated in Figure 5A. To understand the kinetics of the composite, CVs with various scan rates were obtained. Under a lower scan rate (10 mV/s), the electron transfer between electrode−electrolyte interfaces occurs slowly, while upon further increasing, the peak current increases due to the

https://doi.org/10.1021/acsomega.2c01536
ACS Omega 2022, 7, 19754−19763

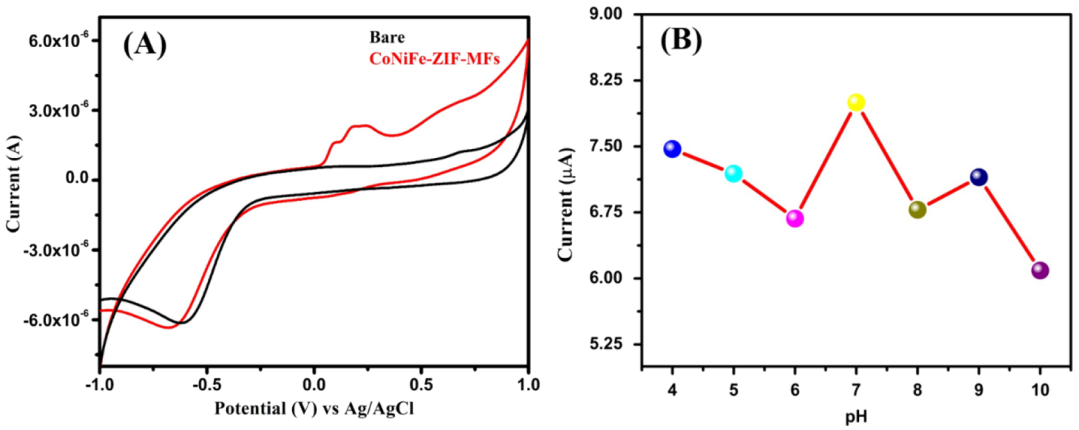

Figure 6. (A) CV for the bare and CoNiFe-ZIF-MFs-modified GCEs in PBS (7.0) and (B) effect of different pH values from 4 to 10 in the same setup for CoNiFe-ZIF-MFs.

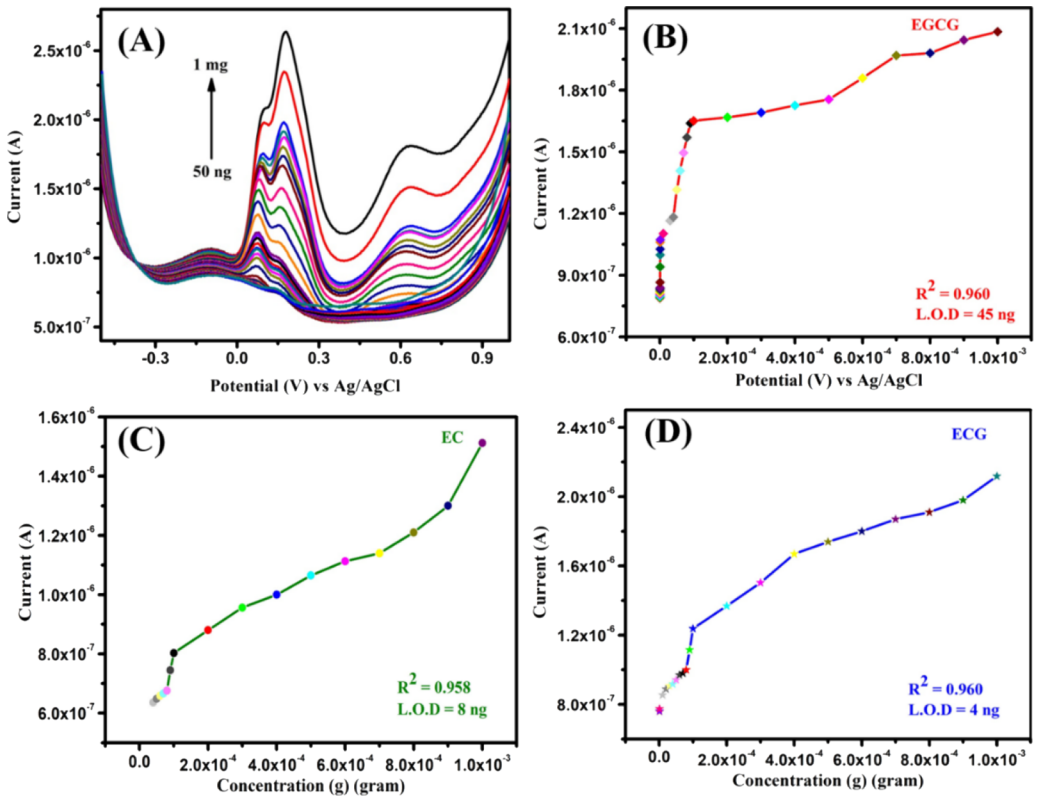

Figure 7. (A) SWV results of the CoNiFe-ZIF-MFs-modified GCE in PBS (7.0) of amounts ranging from 50 ng to 1 mg and (B–D) calibration plot obtained for the three CTs.

rapid diffusion of ions. This confirms that the redox reaction of the composite is the diffusion-controlled process Figure S1A,B. The peak potential difference (ΔE_p) values are higher than 59 mV at higher scan rates, representing the whole system as a quasi-reversible system.[28] This is also supported by the linear plot fitted for the peak current *vs* different scan rates. Further, the electrochemical surface area of the CoNiFe-ZIF-MFs composite is determined using the equation $ip = 2.69 \times 10^5 \times (AD)^{1/2} \times n^{3/2} \times C \times v^{1/2}$ as 37.76 cm^{-2}, which is very high when compared to those of the bimetallic ZIFs (23.24 cm^{-2} for CoFe-ZIF-MFs and 10.20 cm^{-2} for NiFe-ZIF-MFs). These values also confirm the high surface area of the composite, with the related calculation given as Section S1 in the SI and the CV analysis of the bimetallic ZIFs also shown as Figure S2.

Similarly, the resistance of the material should also be determined since it affects the electrochemical activity directly. So, the resistivity of the composite-modified and unmodified GCEs is determined. Generally, EIS is one of the prominent domain used in electrochemistry to describe the electrode by charge transfer resistances of the solution and electrode materials.[28] From the results in Figure 5B, the composite shows a higher peak than the bare GCE, suggesting that its resistance is a little bit higher. This is already confirmed above as the result of the ferrous ion and PAN in the ZIF matrix. The charge transfer resistance (R_{ct}) values are calculated using Randles equivalent circuit as 520 Ωcm^{-2} and 680 Ωcm^{-2} for

https://doi.org/10.1021/acsomega.2c01536
ACS Omega 2022, 7, 19754−19763

Table 1. Comparison of Various Modified Electrodes and Methods toward Different CT Sensing[a]

S. No	method	electrode	analyte biomolecule			range of detection (μM)	limit of detection (μM)			reference
	electrochemical	MIP-Q@G electrode	EC			1−500	0.33			29
		poly(pyromelliticdianhydride-*co*-thionin)	EC			50−300	18			30
		Pt/MnO_2/f-MWCNT-modified GCE	EC			2−9500	0.02			31
		MIP/GO/GCE	EGCG			0.03−10	0.008			32
		molecularly imprinted poly(*o*-phenylenediamine) film	EGCG			50−10,000	160			33
		OPFP-CPE	EGCG			50−125	13.2			34
		$Ni(OH)_2$-modified MIP	EGCG			10−100	0.007			13
		GCE	EGCG			0.1−1	0.065			35
	HPLC	borate−phosphate−SDS-based MEKC	EGCG	EC	ECG		0.192	0.321	0.040	6
	fluorescence	graphene quantum dots				0.01−30	0.005			7
	liquid chromatography method with multichannel electrochemical detection	four channel detector with glassy carbon electrodes	EGCG			0.015−2.5	0.006			36
	adsorptive stripping voltammetry	Pt/PEDOT-modified electrodes	EC			0.2 to 2.5 ppm	0.09 ppm			37
	electrochemical	CoNiFe-ZIF-MFs	EGCG	EC	ECG	0.05−1000	0.045	0.008	0.004	present work

[a]MIP-Q@G electrode: molecular imprinted polymer-quercetin @ graphite electrode; Pt/MnO_2/f-MWCNT-modified GCE: platinum nanoparticle-coated manganese dioxides@multiwalled carbon nanotubes; MIP/GO/GCE: molecular imprinted polymer/graphene oxide/glassy carbon electrode; OPFP-CPE: *n*-octylpyridiniumhexafluorophosphate-carbon paste electrode; $Ni(OH)_2$-modified MIP: nickel hydroxide-modified molecular imprinted polymer; borate−phosphate−SDS-based MEKC: borate−phosphate−sodium dodecyl sulfate-based MEKC; Pt/PEDOT-modified electrodes: platinum/poly(3,4-ethylenedioxythiophene)-modified electrodes.

the bare and composite-modified GCEs, respectively. This is in accordance with their obtained CV values, proving its conductivity in $[Fe(CN)_6]^{3-/4-}$ medium.

3.2.2. Electrochemical Behavior of the Composite in the GT Extract Detection along with Scan Rate Studies and pH Effect. The detection of CTs is investigated using a CV study with 100 μg of GT extract. The potential is kept in a wide range of −1 to 1 V to check the possible interacting compounds in the GT. So, fixing this as the optimum range, the experiment was conducted, in which the composite-modified electrode showed a maximum current value when compared with the unmodified GCE, which confirmed the superior detection efficiency (Figure 6A). Interestingly, three peaks are obtained at potentials 0.09, 0.17, and 0.63 V, suggesting that some of the CTs present in the GT extract are detected by the composite. To validate the obtained results of GT extract, CV analysis with the commercially collected EC and EGCG samples was performed, shown in Figure S3. These studies confirm the oxidation values corresponding to EC, EGCG, and ECG in both GT and the commercial samples, which is also verified with the literature.[13,12] All these three CTs contribute as the major compounds in this group; so, their detection is very much important to estimating the quality of GT. This interaction arises owing to the electrostatic attraction of metal ions on the composite surface with the OH^- groups of the detected CTs in GT. All the three CTs have a similar structure except the change in their primary hydroxyl group number. The peak currents obtained for the composite in the presence of GT are 1.631, 2.31, and 3.221 μA. The trimetal ions, which are distributed equally on the composite surface, can efficiently interact with the CTs of GT, producing sensitive and selective results. Similarly, to determine the process involved, the system is subjected to the same setup as mentioned above (Section 3.2.1) and results are shown in Figure S4A. This also implies that the entire reaction happened because of the diffusion-controlled process supported by the linear plots in Figure S4B−D.

3.2.3. Effect of pH. The pH of PBS is very much involved in determining the CTs and plays a vital role in the sensing behavior. Figure 6B shows the CVs recorded for different pH values ranging 4−10 with 100 μL of GT extract. The obtained results clearly depict that except for pH 7, all other pH values have lower current values. This may be attributed to the following reasons: (i) In acidic medium, all the obtained H^+ ions will electrostatically repel against the metal ions, hindering their binding affinity with GT. (ii) In basic medium, the larger quantity of OH^- groups will readily form the same electrostatic repulsion with GT, thereby reducing their interaction with the electrolyte, which is the reason for their low performance. But, in neutral pH, these effects are neutralized and so the effective binding of GT and CoNiFe-ZIF-MFs composite occurred in the PBS electrolyte at pH 7. Considering these reasons and the obtained results, the pH 7 is used for other experiments.

3.2.4. Square Wave Voltammetry Study. To determine the sensitivity of the electrode toward GT detection, it is subjected to quantify the GT extract in 10 mL of PBS (pH 7). The concentration of the GT extract is added from 50 ng to 1 mg using a standard addition method, and the results are presented in Figure 7A−D. In Figure 7A, we can observe the three peaks emerging due to the interaction of CTs in GT with the composite, exhibiting the sensing of EGCG, EC, and ECG. A further increase in their concentrations has increased the peak currents. This is mainly due to the highly porous nature of the composite, providing a pathway for effective interaction with the GT. As said earlier, all these three analytes have the same structure but vary in the number of hydroxyl groups present in them. So, the necessary interhydrogen bonding formed may result in the interaction with 2-methylimiadazole

https://doi.org/10.1021/acsomega.2c01536
ACS Omega 2022, 7, 19754−19763

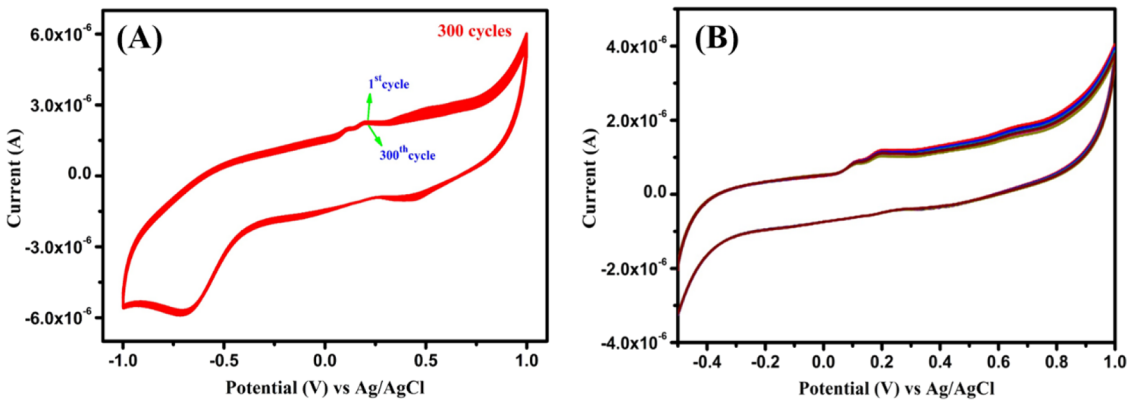

Figure 8. (A) Stability of the CoNiFe-ZIF-MFs composite for 300 cycles in CV at 50 mV/s. (B) Reproducibility of the composite on four different GCE electrodes.

or with the polymeric network. This suggests that the usage of PAN may reduce the crystalline nature of the composite but is very much useful for interaction with biomolecules, thereby increasing the performance of the composite. Along with this, the electrostatic attraction between the Fe^{3+} ions in the composite and the OH groups of the CTs also provided necessary interaction. By the experimental results under optimal conditions, the SWV data exhibited a linear increase in peak currents with the increase in GT concentrations. The slight peak shift observed for all the three CTs toward the higher potential side arises as a result of the accumulation of higher amounts of analytes in high concentrations, which makes the composite require more binding potential to attach them. From Figure 6B–D, the linear regression equations I (μA) and detection limit are obtained as $y = 9.0287x \times 10^{-4} + 1.2230 \times 10^{-6}$ with 45 ng and $R^2 = 0.960$ for EGCG, $y = 6.7028x \times 10^{-4} + 7.2923 \times 10^{-7}$ with 8 ng and $R^2 = 0.958$ for EC, and $y = 7.7929x \times 10^{-4} + 6.5111 \times 10^{-7}$ with 4 ng and $R^2 = 0.956$ for ECG. The sensitivity values are obtained as 23.90, 17. 74, and 20.63 $\mu A \cdot M^{-1}$ cm^{-2} for all the three CTs. The results confirm the impressive electrochemical performance of the proposed CoNiFe-ZIF-MFs-modified electrode with satisfactory results in detection limit and sensitivity in the detection of GT extract. As reported earlier, the Fe ions were more superior to other transition metal ions and they must be involved in the GT sensing compared with the Co and Ni ions.[26] On the other hand, in the case of fluorescence spectra studies, Co ions lead from the front showing an emission peak as they have strong a d–d transition compared to the other two metal ions. The peak currents increased linearly but showed some loss of uniformity, which is clearly seen in the linear plots of all the three CTs, caused by the role of minor matrix effects. In spite of these, the detection limits, sensitivities, and a wide linear range obtained for this proposed biosensor make it an acceptable candidate for further device fabrications. The literature survey with the existing reports on CT sensing using a variety of techniques is shown in Table 1. Here, all the CTs used are commercially purchased and they exhibited a significant LOD. However, using the raw form of GT, we have demonstrated the LOD in an excellent manner, which proposes the efficiency of the composite as an alternative material for simultaneous detection of GT.

3.2.5. Stability and Reproducibility of CoNiFe-ZIF-MFs. Bringing a lab to land approach, stability is also a main parameter to be addressed. To determine this, the CoNiFe-ZIF-MFs composite is subjected to 300 cycles with 100 μL of GT. Surprisingly, the result exhibited consistent peaks, confirming its stable redox process holding up to 87% of its initial current in the 300th cycle (Figure 8A). Incorporation of PAN in the preparation of the ZIF fibrous network strongly binds the metal ions attached on the surface along with the 2-methyimidazole matrix, thereby leading to this highly stable composite. This confirms the cycling stability of the composite, which is suggested for further real-sample analysis.

The reproducibility of CoNiFe-ZIF-MFs@GCE is exhibited using CV for four composite-coated GCEs with 100 μL of GT extract. Here, Figure 8B shows the different electrode responses, confirming the anti-fouling nature of the proposed biosensor with 3.8% RSD value. This characteristic feature too holds evidence for this composite as an efficient material for device fabrications.

4. CONCLUSIONS

Herein, an attempt has been made to detect the CTs in GT extract in its raw form using the electrochemical method. To achieve this, a trimetal ZIF matrix of microfibers is synthesized successfully by employing a simple wet chemical and electrospinning method. Primary characterizations confirmed the material formation, and the basic electrochemical measurements showed the superior conductivity of the CoNiFe-ZIF-MFs composite. Further, SWV studies proved the composite sensitivity in simultaneous sensing of all the three CTs in a linear range of 50 ng to 1mg with detection limits as 45, 8, and 4 ng. From the satisfactory results obtained, the proposed composite has the ability to detect the CTs in natural GT extract simultaneously, whereas to the best of our knowledge, no other works have been done so far using the electrochemical method especially. So, compiling all these results and suggestion, we recommend this CoNiFe-ZIF-MFs biosensor for miniaturized health care device fabrication.

■ ASSOCIATED CONTENT

Supporting Information

The Supporting Information is available free of charge at https://pubs.acs.org/doi/10.1021/acsomega.2c01536.

Different scan rate studies on $[Fe(CN)_6]^{3-/4-}$ solution and PBS along with their linear fits, CV analysis of different bimetallic (CoFe and NiFe) composites with the trimetallic CoNiFe-ZIF-MFs in 100 μL of GT extract, CV analysis of CoNiFe-ZIF-MFs with and

https://doi.org/10.1021/acsomega.2c01536
ACS Omega 2022, 7, 19754–19763

without the presence of GT extract, and electrochemical surface area calculation (PDF)

AUTHOR INFORMATION

Corresponding Authors

Subrata Kundu − *Electrochemical Process Engineering (EPE) Division, CSIR-Central Electrochemical Research Institute (CECRI), Karaikudi, Tamil Nadu 630003, India;* orcid.org/0000-0002-1992-9659; Email: skundu@cecri.res.in

Jeyaraj Wilson − *Polymer Electronics Laboratory, Department of Bioelectronics and Biosensors, Alagappa University, Karaikudi, Tamil Nadu 630 003, India;* orcid.org/0000-0002-2260-4986; Email: wilson.j2008@yahoo.com

Authors

Thatchanamoorthy Thenrajan − *Polymer Electronics Laboratory, Department of Bioelectronics and Biosensors, Alagappa University, Karaikudi, Tamil Nadu 630 003, India;* orcid.org/0000-0002-9102-7860

Sam Sankar Selvasundarasekar − *Electrochemical Process Engineering (EPE) Division, CSIR-Central Electrochemical Research Institute (CECRI), Karaikudi, Tamil Nadu 630003, India;* orcid.org/0000-0003-2262-7739

Complete contact information is available at: https://pubs.acs.org/10.1021/acsomega.2c01536

Author Contributions

[¥]T.T. and S.S.S. contributed equally.

Notes

The authors declare no competing financial interest.

ACKNOWLEDGMENTS

The author J.W. gratefully acknowledges the RUSA 2.0 [F.24-51/2014-U, Policy (TN Multi-Gen), Dept. of. Edn, Gol] for financial assistance. CSIR-CECRI Manuscript reference Number: CECRI/PESVC/Pubs/2022-034.

REFERENCES

(1) Fernandes, S. C.; Osório, R. E. H. M.; Anjos, A.; Neves, A.; Micke, G. A.; Vieira, I. C. Determination of Catechin in Green Tea Using a Catechol Oxidase Biomimetic Sensor. *J. Braz. Chem. Soc.* **2008**, *19*, 1215−1223.

(2) Yang, C. C.; Wu, C. J.; Chien, C. Y.; Chien, C. T. Green Tea Polyphenol Catechins Inhibit Coronavirus Replication and Potentiate the Adaptive Immunity and Autophagy-Dependent Protective Mechanism to Improve Acute Lung Injury in Mice. *Antioxidants* **2021**, *10*, 1−19.

(3) Robb, C. S.; Geldart, S. E.; Seelenbinder, J. A.; Brown, P. R. Analysis of Green Tea Constituents by HPLC-FTIR. *J. Liq. Chromatogr. Relat. Technol.* **2002**, *25*, 787−801.

(4) Friedman, M.; Levin, C. E.; Choi, S. H.; Kozukue, E.; Kozukue, N. HPLC Analysis of Catechins, Theaflavins, and Alkaloids in Commercial Teas and Green Tea Dietary Supplements: Comparison of Water and 80% Ethanol/Water Extracts. *J. Food Sci.* **2006**, *71*, 328−337.

(5) Wang, H.; Helliwell, K.; You, X. Isocratic Elution System for the Determination of Catechins, Caffeine and Gallic Acid in Green Tea Using HPLC. *Food Chem.* **2000**, *68*, 115−121.

(6) Bonoli, M.; Pelillo, M.; Toschi, T. G.; Lercker, G. Analysis of Green Tea Catechins: Comparative Study between HPLC and HPCE. *Food Chem.* **2003**, *81*, 631−638.

(7) Sun, J.; He, Y.; Wang, L. Enzyme-Free Fluorescence Sensing of Catechins in Green Tea Using Bifunctional Graphene Quantum Dots. *Anal. Methods* **2017**, *9*, 3525−3530.

(8) Du, C.; Ma, C.; Gu, J.; Li, L.; Zhu, C.; Chen, L.; Wang, T.; Chen, G. Rapid Determination of Catechin Content in Black Tea by Fluorescence Spectroscopy. *J. Spectrosc.* **2020**, *2020*, 1.

(9) Lee, J. M.; Karim, M. M.; Lee, S. H. Determination of Catechin in Aqueous Solution by Chemiluminescence Method. *J. Fluoresc.* **2005**, *15*, 735−739.

(10) Apak, R.; Demirci Çekiç, S.; Çetinkaya, A.; Filik, H.; Hayvali, M.; Kiliç, E. Selective Determination of Catechin among Phenolic Antioxidants with the Use of a Novel Optical Fiber Reflectance Sensor Based on Indophenol Dye Formation on Nano-Sized TiO 2. *J. Agric. Food Chem.* **2012**, *60*, 2769−2777.

(11) Grieshaber, D.; MacKenzie, R.; Vörös, J.; Reimhult, E. Electrochemical Biosensors - Sensor Principles and Architectures. *Sensors* **2008**, *8*, 1400−1458.

(12) Chatterjee, T. N.; Das, D.; Roy, R. B.; Tudu, B.; Sabhapondit, S.; Tamuly, P.; Pramanik, P.; Bandyopadhyay, R. Molecular Imprinted Polymer Based Electrode for Sensing Catechin (+C) in Green Tea. *IEEE Sens. J.* **2018**, *18*, 2236−2244.

(13) Nandy Chatterjee, T.; Das, D.; Banerjee Roy, R.; Tudu, B.; Hazarika, A. K.; Sabhapondit, S.; Tamuly, P.; Bandyopadhyay, R. Development of a Nickel Hydroxide Nanopetal Decorated Molecular Imprinted Polymer Based Electrode for Sensitive Detection of Epigallocatechin-3-Gallate in Green Tea. *Sens. Actuators, B* **2019**, *283*, 69−78.

(14) Stassen, I.; Styles, M.; Grenci, G.; Van Gorp, H.; Vanderlinden, W.; De Feyter, S.; Falcaro, P.; De Vos, D.; Vereecken, P.; Ameloot, R. Chemical Vapour Deposition of Zeolitic Imidazolate Framework Thin Films. *Nat. Mater.* **2016**, *15*, 304−310.

(15) Sharma, G.; Kumar, D.; Kumar, A.; Al-Muhtaseb, A. H.; Pathania, D.; Naushad, M.; Mola, G. T. Revolution from Monometallic to Trimetallic Nanoparticle Composites, Various Synthesis Methods and Their Applications: A Review. *Mater. Sci. Eng. C* **2017**, *71*, 1216−1230.

(16) Sankar, S. S.; Karthick, K.; Sangeetha, K.; Karmakar, A.; Kundu, S. Polymeric Nanofibers Containing CoNi-Based Zeolitic Imidazolate Framework Nanoparticles for Electrocatalytic Water Oxidation. *ACS Appl. Nano Mater.* **2020**, *3*, 4274−4282.

(17) Thenrajan, T.; Sankar, S. S.; Srinivasan, G.; Kundu, S.; Wilson, J. Cobalt−Iron Zeolitic Imidazolate Frameworks (ZIFs) as Microfibers for the Effective Detection of Hydroquinone. *Dalt. Trans.* **2021**, *50*, 10540−10548.

(18) Thenrajan, T.; Sankar, S. S.; Kundu, S.; Wilson, J. Bimetallic Nickel Iron Zeolitic Imidazolate Fibers as Biosensing Platform for Neurotransmitter Serotonin. *Colloid Polym. Sci.* **2022**, 223.

(19) Furukawa, H.; Cordova, K. E.; O'Keeffe, M.; Yaghi, O. M. The Chemistry and Applications of Metal-Organic Frameworks. *Science* **2013**, *341*, 1230444.

(20) Kaur, G.; Rai, R. K.; Tyagi, D.; Yao, X.; Li, P. Z.; Yang, X. C.; Zhao, Y.; Xu, Q.; Singh, S. K. Room-Temperature Synthesis of Bimetallic Co-Zn Based Zeolitic Imidazolate Frameworks in Water for Enhanced CO2 and H2 Uptakes. *J. Mater. Chem. A* **2016**, *4*, 14932−14938.

(21) Sankar, S. S.; Karthick, K.; Sangeetha, K.; Karmakar, A.; Madhu, R.; Kundu, S. Current Perspectives on 3D ZIFs Incorporated with 1D Carbon Matrices as Fibers via Electrospinning Processes towards Electrocatalytic Water Splitting: A Review. *J. Mater. Chem. A* **2021**, *9*, 11961−12002.

(22) Zhao, G.; Wu, H.; Feng, R.; Wang, D.; Xu, P.; Wang, H.; Guo, Z.; Chen, Q. Bimetallic Zeolitic Imidazolate Framework as an Intrinsic Two-Photon Fluorescence and PH-Responsive MR Imaging Agent. *ACS Omega* **2018**, *3*, 9790−9797.

(23) Abuzalat, O.; Wong, D.; Park, S. S.; Kim, S. Highly Selective and Sensitive Fluorescent Zeolitic Imidazole Frameworks Sensor for Nitroaromatic Explosive Detection. *Nanoscale* **2020**, *12*, 13523−13530.

https://doi.org/10.1021/acsomega.2c01536
ACS Omega 2022, 7, 19754−19763

(24) Sankar, S. S.; Manjula, K.; Keerthana, G.; Ramesh Babu, B.; Kundu, S. Highly Stable Trimetallic (Co, Ni, and Fe) Zeolite Imidazolate Framework Microfibers: An Excellent Electrocatalyst for Water Oxidation. *Cryst. Growth Des.* **2021**, 1800.
(25) Schejn, A.; Aboulaich, A.; Balan, L.; Falk, V.; Lalevée, J.; Medjahdi, G.; Aranda, L.; Mozet, K.; Schneider, R. Cu2+-Doped Zeolitic Imidazolate Frameworks (ZIF-8): Efficient and Stable Catalysts for Cycloadditions and Condensation Reactions. *Catal. Sci. Technol.* **2015**, *5*, 1829−1839.
(26) Sun, L.; Hendon, C. H.; Park, S. S.; Tulchinsky, Y.; Wan, R.; Wang, F.; Walsh, A.; Dincă, M. Is Iron Unique in Promoting Electrical Conductivity in MOFs? *Chem. Sci.* **2017**, *8*, 4450−4457.
(27) Elgrishi, N.; Rountree, K. J.; McCarthy, B. D.; Rountree, E. S.; Eisenhart, T. T.; Dempsey, J. L. A Practical Beginner's Guide to Cyclic Voltammetry. *J. Chem. Educ.* **2018**, *95*, 197−206.
(28) Bojang, A. A.; Wu, H. S. Characterization of Electrode Performance in Enzymatic Biofuel Cells Using Cyclic Voltammetry and Electrochemical Impedance Spectroscopy. *Catalysts* **2020**, *10*, 782.
(29) Kishore Kumar, D.; Raghava Reddy, K.; Sadhu, V.; Shetti, N. P.; Venkata Reddy, C.; Chouhan, R. S.; Naveen, S. Metal Oxide-Based Nanosensors for Healthcare and Environmental Applications. *Nanomater. Diagn. Tools Devices.* **2020**, 113−129.
(30) Duran, S. T. Research Article Preparation Of Poly (Pyromellitic Dianhydride-Co- Thionin) Modified Voltammetric Sensor For The Determination Of Epicatechin. *J. Turk. Chem. Soc., Sect. A* **2018**, *5*, 1021−1028.
(31) Ezhil Vilian, A. T.; Madhu, R.; Chen, S. M.; Veeramani, V.; Sivakumar, M.; Huh, Y. S.; Han, Y. K. Facile Synthesis of MnO2/Carbon Nanotubes Decorated with a Nanocomposite of Pt Nanoparticles as a New Platform for the Electrochemical Detection of Catechin in Red Wine and Green Tea Samples. *J. Mater. Chem. B* **2015**, *3*, 6285−6292.
(32) Liu, Y.; Zhu, L.; Hu, Y.; Peng, X.; Du, J. A Novel Electrochemical Sensor Based on a Molecularly Imprinted Polymer for the Determination of Epigallocatechin Gallate. *Food Chem.* **2017**, *221*, 1128−1134.
(33) Duan, Y.; Luo, X.; Qin, Y.; Zhang, H.; Sun, G.; Sun, X.; Yan, Y. Determination of Epigallocatechin-3-Gallate with a High-Efficiency Electrochemical Sensor Based on a Molecularly Imprinted Poly(o-Phenylenediamine) Film. *J. Appl. Polym. Sci.* **2013**, *129*, 2882−2890.
(34) Fan, K.; Luo, X.; Ping, J.; Tang, W.; Wu, J.; Ying, Y.; Zhou, Q. Sensitive Determination of (−)-Epigallocatechin Gallate in Tea Infusion Using a Novel Ionic Liquid Carbon Paste Electrode. *J. Agric. Food Chem.* **2012**, *60*, 6333−6340.
(35) Novak, I.; Šeruga, M.; Komorsky-Lovrić, Š. Electrochemical Characterization of Epigallocatechin Gallate Using Square-Wave Voltammetry. *Electroanalysis* **2009**, *21*, 1019−1025.
(36) Long, H.; Zhu, Y.; Cregor, M.; Tian, F.; Coury, L.; Kissinger, C. B.; Kissinger, P. T. Liquid Chromatography with Multi-Channel Electrochemical Detection for the Determination of Epigallocatechin Gallate in Rat Plasma Utilizing an Automated Blood Sampling Device. *J. Chromatogr. B Biomed. Sci. Appl.* **2001**, *763*, 47−51.
(37) Pigani, L.; Seeber, R.; Bedini, A.; Dalcanale, E.; Suman, M. Adsorptive-Stripping Voltammetry at PEDOT-Modified Electrodes. Determination of Epicatechin. *Food Anal. Methods* **2014**, *7*, 754−760.

https://doi.org/10.1021/acsomega.2c01536
ACS Omega 2022, 7, 19754−19763